NJC

PAPER

View Article Online
View Journal | View Issue

Cite this: *New J. Chem.*, 2019, **43**, 16583

Bimetallic Co/Al nanoparticles in an ionic liquid: synthesis and application in alkyne hydrogenation†

Laura Schmolke,[a] Bernhard J. Gregori,[b] Beatriz Giesen,[a] Alexa Schmitz,[a] Juri Barthel,[c] Lena Staiger,[d] Roland A. Fischer,[d] Axel Jacobi von Wangelin *[b] and Christoph Janiak *[a]

Herein, we report the microwave-induced decomposition of various organometallic cobalt and aluminum precursors in an ionic liquid (IL), 1-butyl-3-methylimidazolium bis(trifluoromethylsulfonyl)imide ([BMIm]NTf$_2$), resulting in Co/Al nanoalloys with different molar Co/Al ratios. The dual-source precursor system of dicobalt octacarbonyl ($Co_2(CO)_8$) and pentamethylcyclopentadienyl aluminum ([AlCp*]$_4$) in [BMIm]NTf$_2$ afforded CoAl nanoparticles (CoAl-NPs) with a molar Co/Al ratio of 1 : 1. Their size and size distribution were determined *via* transmission electron microscopy (TEM) to be an average diameter of 3.0 ± 0.5 nm. Furthermore, the dual-source precursor system of cobalt amidinate ([Co(^{i}Pr$_2$-MeAMD)$_2$]) and aluminum amidinate [Me$_2$Al(^{i}Pr$_2$-MeAMD)] in molar ratios of 1 : 1 and 3 : 1 resulted in CoAl- and Co_3Al-NPs with an average diameter of 3 ± 1 and 2.0 ± 0.2 nm, respectively. All the obtained materials were characterized *via* TEM, energy dispersive X-ray spectroscopy (EDX), selected area electron diffraction (SAED), together with high-angle annular dark-field scanning transmission electron microscopy (HAADF-STEM) and (high-resolution) X-ray photoelectron spectroscopy ((HR-)XPS). Phase-pure Co/Al-NPs were not obtained since the concomitant formation of Co-NPs and Al_2O_3 occurred in this wet-chemical synthesis. The as-prepared Co/Al nanoalloys were evaluated as catalysts in the hydrogenation of phenylacetylene under mild conditions (2 bar H_2, 30 °C in THF). In comparison to the monometallic Co-NPs, the Co/Al-NPs showed a significantly higher catalytic hydrogenation activity. The Co- and Co/Al-NPs were also active under harsher reaction conditions (80 bar H_2, 80 °C) without the addition of the activating co-catalyst DIBAL-H.

Received 12th July 2019,
Accepted 23rd September 2019

DOI: 10.1039/c9nj03622a

rsc.li/njc

Introduction

Nanoalloys are a promising class of catalysts due to their modular composition of metallic components and surface characteristics, shapes, and sizes.[1–4] One of the first applied bimetallic catalysts was the Lindlar catalyst for the semi-hydrogenation of alkynes.[5] The Lindlar catalyst consists of 4–6% Pd on calcium carbonate with lead acetate as a poison to prevent full hydrogenation.[6,7] The catalyst is still important for industrial processes such as the synthesis of vitamin A.[8] The vast majority of bimetallic catalysts studied in the past decades are combinations of transition metals, typically involving noble metals with non-noble transition or main-group metals (*e.g.* Pd/Ga,[9] Rh/Co,[10] Cu/Co,[11] Pt/Co,[12] and Ru/Co[20]). Non-noble catalysts (*e.g.* Ni/Ga,[13] Cu/Zn,[14] and Fe_4Al_{13}[15]) have attracted considerable interest as low-cost alternatives to noble metal catalysts. The second metal in nanoalloys is generally regarded as a promoter, which modulates the activity and/or selectivity of the catalytically active metal sites.[16] Promotors can increase the turnover frequency (NiPd/C[17]), modify the selectivity of a certain catalytic reaction (Lindlar catalyst[5]) and improve the catalyst stability (Co/Pt-NPs[18]).[23] For example, the alloying of Pt nanocatalysts with Sn enables the selective hydrogenation of cinnamic aldehyde to α,β-unsaturated cinnamic alcohol.[19] Bimetallic transition metal Co/M-nanoparticle systems (Co/M = Co/Mn,[20] Co/Re,[20] Co/Ni,[21] Co/Fe[21] and the previously noted noble-metal/cobalt-nanoalloys) are well known as catalysts for the Fischer–Tropsch process.

Nanoalloys of non-noble transition metals with the electropositive main-group metals Al or Ga are far less explored.[22–24]

[a] *Institut für Anorganische Chemie und Strukturchemie, Heinrich-Heine-Universität Düsseldorf, D-40225 Düsseldorf, Germany. E-mail: janiak@uni-duesseldorf.de; Fax: +49-211-81-12287; Tel: +49-211-81-12286*
[b] *Institut für Anorganische und Angewandte Chemie, Universität Hamburg, 20146 Hamburg, Germany. E-mail: axel.jacobi@chemie.uni-hamburg.de*
[c] *Ernst Ruska-Centrum für Mikroskopie und Spektroskopie mit Elektronen (ER-C 2), Forschungszentrum Jülich GmbH, D-52425 Jülich, Germany*
[d] *Department of Chemistry, Technische Universität München, D-85748 Garching, Germany*

† Electronic supplementary information (ESI) available: IL and precursor analysis TEM images with particle size histograms, SAEDs, EDX and XPS analysis, details of the hydrogenation reactions. See DOI: 10.1039/c9nj03622a

For example, Cokoja *et al.* reported the synthesis of CoAl,[25] NiAl,[26] $CuAl_x$ (x = 1 and 2)[27] and CuE_2 (E = Al and Ga)[28] nanoparticles *via* the wet-chemical hydrogenolysis of all-hydrocarbon precursors in organic solvents. Schütte *et al.* prepared NiGa-, Ni_2Ga_3- and Ni_3Ga-NPs as noble metal-free catalysts for the semi-hydrogenation of alkynes.[13] The preparation of well-defined Co/Al-nanoalloys has largely been under-utilized and their catalytic properties are unknown. However, CoAl can be viewed as a lighter and inexpensive homologue of the already reported Ni/Ga[13] and Pd/Ga[9] nanoalloys.

The preparation of especially small (<5 nm) nanoalloys bears great potential for catalytic application due to their high dispersion in organic solvents and high surface-to-volume ratio with a potentially high number of active sites. However, these small nanoparticles may also undergo rapid agglomeration and aggregation.[29,30] Thus, to prevent such deactivation, ionic liquids (ILs) have been employed as appropriate solvents and stabilizing reagents in the synthesis and catalytic application of metal nanoparticles (M-NPs).[31–35]

There is considerable interest in the application of bimetallic nanomaterials in ionic liquids in catalysis.[36] For example, bimetallic Pd/Au-NPs in imidazolium ionic liquids showed higher activity for hydrogenation reactions of different substrates than monometallic Pd-NPs.[37]

Electrostatic and steric interactions of ILs, which are otherwise only weakly-coordinating, stabilize M-NPs with little change in their surface properties.[38–41] Furthermore, the high ionic charge, polarity and dielectric constant of ILs result in excellent microwave absorption efficiencies, which enable effective heating by microwave irradiation.[42–44]

Metal amidinates and metal carbonyls are well established as (organometallic) precursors in the soft and wet-chemical synthesis of M-NPs.[45–51] They exhibit decomposition temperatures below 200 °C and their gaseous decomposition products are easily removed so that product contamination is minimized.[52–57] Monometallic Co-NPs have been applied in catalytic hydrogenation reactions[58] of various substrates such as nitriles,[59] ketones and aldehydes,[60,61] alkynes[62,63] and alkenes,[64] albeit their activity is low in comparison with *e.g.* Ni-NPs under similar conditions.[65] Moreover, Fe-NPs are known photoactive catalysts for the hydrogenation of alkynes and alkenes.[66] Metallic Co/Al-NPs appear to be unknown in catalytic hydrogenation reactions. Wang *et al.* reported $CoAlO_x$-NPs for the catalytic hydrogenation of CO_2 to ethanol.[67]

Herein, we investigate the possibilities to prepare Co/Al-NPs *via* wet-chemical synthesis through the microwave-assisted thermal decomposition of various organometallic cobalt and aluminum complexes in an ionic liquid. The aim of this study is to derive a controllable synthesis route for Co/Al-NPs, which are still difficult to obtain, and to examine their catalytic properties in alkyne hydrogenation reactions (Scheme 1).

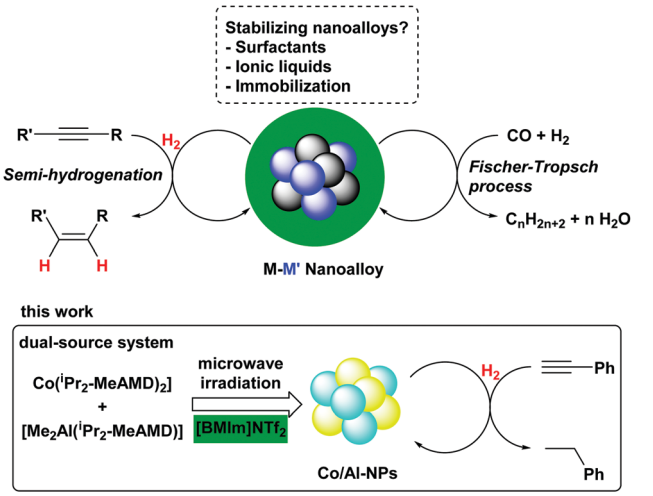

Scheme 1 Wet-chemical synthesis of Co/Al-NPs in $[BMIm]NTf_2$ and their application in alkyne hydrogenation reactions.

Experimental

Materials

All synthetic experiments were carried out under a nitrogen or argon atmosphere using Schlenk techniques since the organometallic precursors and Co/Al-NPs are hygroscopic and air sensitive. Solvents were dried using an MBRAUN Solvent Purification System and stored over molecular sieves. The final water contents were checked by Karl Fischer titration, which did not exceed 5 ppm. 1-Chlorobutane (>99%) and 1-methylimidazole (>99%) were obtained from Sigma Aldrich and purified by fractional distillation, then dried over 4 Å molecular sieves for several days. Cobalt(II) chloride hexahydrate (98%) was obtained from Sigma Aldrich and purified by recrystallization in water and dried under high vacuum (10^{-3} mbar) at 140 °C for serval days to obtain cobalt(II) chloride anhydrous. 1,3-Diisopropylcarbodiimide (>99%), methyllithium solution (1.6 M in diethyl ether) and dicobalt octacarbonyl (>90% Co, moistened with hexane) were purchased from Sigma-Aldrich and used without further purification. Lithium bis(trifluoromethanesulfonyl)imide (99%) was purchased from abcr and used without further purification. The low valent cobalt(II) bis(trimethylsilyl)amide ($[Co(btsa)_2]$) was prepared according to a literature procedure.[68] Furthermore, $[(AlCp^*)_4]$ was prepared according to the literature.[69]

Instrumentation

Coulometric Karl Fischer titration was performed with an ECH/ANALYTIK JENA AQUA 40.00 Karl Fischer titrator. The measurements were performed using the headspace module with a dry sample container and crimp caps (∅ = 20 mm, with PTFE septum). The sample containers and crimp caps were dried at 70 °C for 2 days. The measurements were performed in an oven at a temperature of 170 °C.

All ion chromatographic measurements (IC) were carried out using a Dionex ICS 1100 instrument with suppressed conductivity detection. The suppressor (AERS 500, Dionex) was regenerated with an external water module. The system was equipped with an analytical IonPac AS 22 column from Dionex (4 × 250 mm) with the corresponding guard column AG 22 (4 × 50 mm). The instrument was controlled using the

Chromeleon® software (version 7.1.0.898). The injection volume was 25 μL. The standard eluent used was a 4.5 mmol L^{-1} Na_2CO_3 + 1.0 mmol L^{-1} $NaHCO_3$ mixture with an addition of 30 vol% acetonitrile (ACN).

Thermogravimetric analysis (TGA) was carried out with a Netzsch TG 209 F3 Tarsus, equipped with an Al-crucible at a heating rate of 5 K min^{-1} under an inert atmosphere (N_2).

TEM imaging was performed on an FEI Tecnai G2 F20 electron microscope operated at an accelerating voltage of 200 kV.[70] Digital images were recorded using a Gatan UltraScan 1000P detector. Samples were prepared using 200 μm carbon-coated copper grids or gold grids. The size distribution was determined manually or with the aid of the Gatan DigitalMicrograph software by counting at least 100 individual particles.

TEM-EDX spectroscopy was also performed on the FEI Tecnai G2 F20 with a high-angle energy dispersive X-ray detector providing a resolution of 136 eV or better for Mn K-α radiation. The exposure time of individual EDX spectra was 3 min.

Selected area electron diffraction (SAED) patterns were recorded with an FEI Titan 80–300 TEM[71] operated at an accelerating voltage of 300 kV. The area selection was achieved with a round aperture placed in the first intermediate image plane with a corresponding diameter of 0.64 μm in the object plane. For each acquisition, a sample region with a significant amount of material was placed inside the aperture. The object was illuminated with a wide-spread parallel beam to obtain focused diffraction patterns. The diffraction images were calibrated with Debye–Scherrer patterns recorded from a gold reference sample (S106, Plano GmbH, Wetzlar, Germany).

High-angle annular dark-field scanning transmission electron microscopy (HAADF-STEM) micrographs were taken at room temperature with an FEI Tecnai G2 F20 TEM operated at an accelerating voltage of 200 kV. Samples were deposited on 200 μm carbon-coated gold or copper grids.

X-ray photoelectron spectroscopy, XPS-(ESCA-) measurements were performed with a Fisons/VG Scientific ESCALAB 200X xp-spectrometer, operating at 70–80 °C, a pressure of 7.0×10^{-9} mbar and sample angle of 33°. Spectra were recorded using polychromatic Al-K_α excitation (11 kV, 20 mA) at an emission angle of 0° and were referenced to the carbon 1s orbital with a binding energy of 284.8 eV. Calibration of the XPS was carried out by recording spectra with Al-K_α X-rays from clean samples of copper, silver and gold at 50 eV and 10 eV pass energies and comparison with reference values. Fitting of the experimental XP spectra was done with the CasaXPS program, version 2.3.19PR1.0, Copyright 1999–2018 Casa Software Ltd. Short contact with air during sample transfer to the XPS instrument could not be avoided and may have led to surface oxidation.

Autoclaves for hydrogenation reactions. A high-pressure reactor (Parr®), which was loaded in a glovebox, was used for hydrogenation reactions. Hydrogen gas was purchased from Praxair (99.9992%).

Gas chromatography with flame ionization detector (GC-FID). A HP6890 GC-system with an injector 7683B and an Agilent 7820A system was used for GC-FID analysis. A split-less mode was used for the injection. Column: HP-5, 19091J-413 (30 m × 320 μm × 0.25 μm), carrier gas: nitrogen and internal standard: *n*-pentadecane.

Gas chromatography with mass spectrometry detector (GC-MS). An Agilent 6890 N Network GC-system with a mass detector 5975 MS was used for GC-MS analysis. A split mode was used for the injection. Column: SGE-BPX5 (30 m × 250 μm × 0.25 μm) and carrier gas: hydrogen.

Ionic liquid synthesis

The ionic liquid [BMIm]NTf_2 was synthesized by reacting 1-methylimidazole with 1-chlorobutane to yield [BMIm]Cl. [BMIm]Cl and $LiNTf_2$ reacted to give [BMIm]NTf_2.[79] Following washing with water, the IL was dried under ultra-high vacuum (10^{-7} mbar) at 60 °C for one day. The characterization was carried out by ^{1}H-, ^{13}C- and ^{19}F-NMR. The IL purity was assessed by ion chromatography (Dionex ICS-1100, with IonPac® AS22, 4 × 250 mm column) to be > 99.9% (Fig. S1, ESI†). Its water content by coulometric Karl Fischer titration was less than 10 ppm. ^{1}H-NMR ($CDCl_3$, 300 MHz, 298 K): δ/ppm = 0.95 (t, $^3J_{HH}$ = 7.3 Hz, –CH_3, 3H), 1.36 (h, $^3J_{HH}$ = 7.3 Hz, –CH_2, 2H), 1.84 (q, $^3J_{HH}$ = 7.5 Hz, –CH_2, 2H), 3.93 (s, –CH_3, 3H), 4.16 (t, $^3J_{HH}$ = 7.5 Hz, –CH_2, 2H), 7.3 (q, $^3J_{HH}$ = 2.0 Hz, 2x-CH, 2H), 8.72 (s, –CH_3, 1H). ^{13}C-NMR ($CDCl_3$, 75 MHz, 298 K): δ/ppm = 13.32 (s, C–CH_3), 19.45 (s, C–CH_2–C), 32.04 (s, C–CH_2–C), 36.45 (s, N–CH_3), 50.08 (s, N–CH_2–C), 119.92 (q, CF_3), 122.37 (s, CH═C) 123.80 (s, CH═C), 136.19 (s, N–CH–N). ^{19}F-NMR (without solvent, 41 MHz, 298 K) δ/ppm = −78.4.

Metal precursor synthesis

Lithium amidinate was synthesized *via* the deprotonation and methylation of 1,3-diisopropylcarbodiimide with methyllithium (1.6 mol L^{-1} in diethyl ether). The resulting lithium amidinate was reacted in a salt metathesis reaction with the purified cobalt(II) chloride anhydrous according to the literature (Scheme 2).[54,72] ^{1}H-NMR (C_6D_6, 500.13 MHz, 297 K): δ/ppm = −69 (br, 24H), 301 (br, 6H), 320 (br, 4H).

Aluminum amidinate was synthesized *via* the reaction of 1,3-diisopropylcarbodiimide with trimethylaluminum (2.0 M in hexane) according to the literature (Scheme 3).[73] ^{1}H-NMR ($CDCl_3$, 300 MHz, 297 K) δ/ppm = 3.48 (sept, 2H, $^3J_{HH}$ = 6.3 Hz), 1.85 (s, 3H), 0.97 (d, 12H, $^3J_{HH}$ = 6.1 Hz), –0.88 (s, 6H). ^{13}C-NMR: ($CDCl_3$, 75 MHz, 297 K) δ/ppm = 171.16 (s, CMe), 44.42 (s, $CHMe_2$), 24.63 (s, $CHMe_2$), 10.35 (s, CMe), −10.65 (br, $AlMe_2$).

[$Co(btsa)_2$] (0.301 g, 0.8 mmol) and [AlCp*]$_4$ (0.129 g, 0.8 mmol) were suspended in 10 mL toluene and heated to 80 °C for 3 h. All volatiles were removed under reduced pressure.

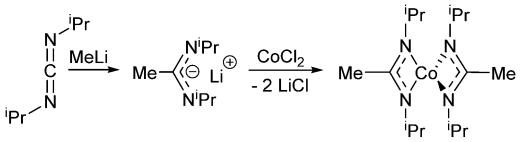

Scheme 2 Synthetic scheme for [Co(^{i}Pr$_2$-MeAMD)$_2$] from 1,3-diisopropylcarbodiimide, methyllithium and cobalt(II) chloride.

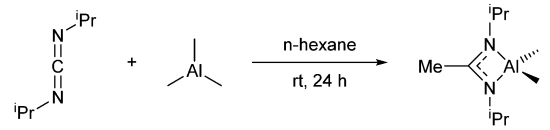

Scheme 3 Synthetic scheme for [$Me_2Al(^iPr_2$-MeAMD)] from 1,3-diisopropylcarbodiimide and trimethylaluminum.

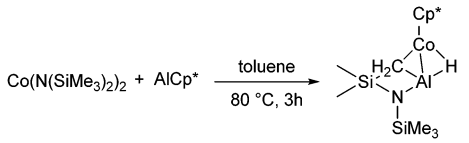

Scheme 4 Synthetic scheme for [Cp*Co(μ-H)(Al(κ^2-(CH_2SiMe_2)NSiMe_3)(btsa))] from [Co(btsa)$_2$] and [AlCp*]$_4$.

The product was recrystallized in *n*-hexane (Scheme 4).[74] ^{1}H-NMR (C_6D_6, 300 MHz rt): δ/ppm = 81.03 (br, s, Cp*), 1.21 (s, btsa), 0.49 (s, btsa), −0.58 (s, btsa). ^{13}C-NMR (C_6D_6, 75 MHz rt): δ/ppm = 9.60–4.34 (overlapping multiplets, btsa).

Metal nanoparticle (M-NP) synthesis

Decomposition by microwave heating was carried out under an argon atmosphere. The masses of the organometallic precursors were set to yield 0.5 or 1.0 wt% Co/Al-NPs in the IL dispersion. The parameters for the microwave-induced M-NP synthesis were modified from the literature procedures.[13,34,45–48,75] All analyses (TEM, STEM, EDX, SAED and XPS) were performed with purified M-NPs. At the chosen temperature of 230 °C, no IL decomposition was seen by TGA, ^{1}H- and ^{19}F-NMR even by holding this temperature for 8 h (Fig. S3, ESI†).

Preparation of CoAl-NPs (NP1). In a microwave vessel, 9 mg (0.055 mmol) [(AlCp*)$_4$] and 10 mg (0.058 mmol) $Co_2(CO)_8$ were dispersed in 1.00 g [BMIm]NTf_2 (to yield 1 wt% Co/Al in the IL dispersion) in a glove box. The yellow dispersion was heated to 65 °C for 5 h and became dark red. After cooling to room temperature, the red dispersion was stirred overnight and then decomposed in a microwave (CEM, Discover) for 30 min at 230 °C (50 W). The dispersion became black, and was then washed with acetonitrile (3 × 2 mL) and centrifuged. The resulting material was dried under high vacuum until a black powder was obtained.

Preparation of CoAl-NPs (NP2). Samples of 56 mg (0.163 mmol) [Co(^{i}Pr$_2$-MeAMD)$_2$] and 32 mg (0.163 mmol) [$Me_2Al(^iPr_2$-MeAMD)] were combined in a microwave vessel in 1.45 g [BMIm]NTf_2 (to yield 1 wt% Co/Al in the IL dispersion) in a glove box. The mixture was stirred for 18 h at room temperature and the resulting black dispersion was decomposed in a microwave (CEM, Discover) for 30 min at 230 °C (50 W). The dispersion became black, and was then washed with acetonitrile (3 × 2 mL) and centrifuged. The resulting material was dried under high vacuum until a black powder was obtained.

Preparation of Co_3Al-NPs (NP3). Samples of 71 mg (0.208 mmol) [Co(^{i}Pr$_2$-MeAMD)$_2$] and 13 mg (0.066 mmol) [$Me_2Al(^iPr_2$-MeAMD)] were combined in a microwave vessel in 1.42 g [BMIm]NTf_2 (to yield 1 wt% Co/Al in the IL dispersion) in a glove box. The mixture was stirred for 18 h at room temperature and the resulting dark dispersion was decomposed in a microwave (CEM, Discover) for 30 min at 230 °C (50 W). The dispersion became black, and was then washed with acetonitrile (3 × 2 mL) and centrifuged. The resulting material was dried under high vacuum until a black powder was obtained.

Preparation of CoAl/Co_3Al-NPs (NP4). Samples of 61 mg (0.178 mmol) [Co(^{i}Pr$_2$-MeAMD)$_2$] and 26 mg (0.131 mmol) [$Me_2Al(^iPr_2$-MeAMD)] were combined in a microwave vessel in 1.35 g [BMIm]NTf_2 (to yield 1 wt% Co/Al in the IL dispersion) in a glove box. The mixture was stirred for 16 h at room temperature and the resulting dark dispersion was decomposed in a microwave (CEM, Discover) for 30 min at 230 °C (50 W). The dispersion became black, and was then washed with acetonitrile (3 × 2 mL) and centrifuged. The resulting material was dried under high vacuum until a black powder was obtained.

Preparation of Co-NPs (NP5). Samples of 27 mg (0.077 mmol) [Co(^{i}Pr$_2$-MeAMD)$_2$] and 14 mg (0.087 mmol) [(AlCp*)$_4$] were combined in a microwave vessel in 1.37 g [BMIm]NTf_2 (to yield 0.5 wt% Co/Al in the IL dispersion) in a glove box. The mixture was stirred overnight at room temperature and the resulting dark dispersion was decomposed in a microwave (CEM, Discover) for 30 min at 230 °C (50 W). The dispersion became black, and was then washed with acetonitrile (3 × 2 mL) and centrifuged. The resulting material was dried under high vacuum until a black powder was obtained.

Preparation of Co-NPs (NP6). 9 mg (0.029 mmol) [Cp*Co(μ-H)-(Al(κ^2-(CH_2SiMe_2)N$SiMe_3$)(btsa))] were suspended in a microwave vessel in 0.49 g [BMIm]NTf_2 (to yield 0.5 wt% Co/Al in the IL dispersion) in a glove box. The mixture was stirred overnight at room temperature and the resulting dark dispersion was decomposed in a microwave (CEM, Discover) for 30 min at 230 °C (50 W). The dispersion became black, and was then washed with acetonitrile (3 × 2 mL) and centrifuged. The resulting material was dried under high vacuum until a black powder was obtained.

Preparation of Co-NPs (NP7). 236 mg (0.690 mmol) [Co(^{i}Pr$_2$-MeAMD)$_2$] (to yield 1 wt% Co in the IL dispersion) were suspended in a microwave vessel in 2.01 g [BMIm]NTf_2 in a glove box. The mixture was stirred overnight at room temperature and the resulting dark dispersion was decomposed in a microwave (CEM, Discover) for 30 min at 230 °C (50 W). The dispersion became black, and was then washed with acetonitrile (3 × 2 mL) and centrifuged. The resulting material was dried under high vacuum until a black powder was obtained.

General procedure for the catalytic hydrogenations with [Co]-NPs

Under an atmosphere of argon (Schlenk technique or glove box), an oven-dried 4 mL vial with a stirring bar was charged with alkyne (0.2 mmol) and *n*-pentadecane as an internal GC reference (0.2 mmol, 42.5 mg). The catalyst (5–10 mol% [Co]-NPs, 10–20 mol% DIBAL-H) and 0.4 mL THF were added and the vial was closed with a septum. The septum was punctured with a short needle and the vial was transferred to a pressure-resistant reactor equipped with a gas inlet. The reactor

was purged with H_2 for 1 min while stirring the reaction mixture. After three short cycles of purging with H_2 by pressurizing and depressurizing (2.0 bar, 5 s, 1.3 bar), the H_2 pressure and temperature were set (2 bar H_2, 30 °C). After 5–16 h, the reactor was cooled, and the pressure released. The vials were retrieved, and saturated aqueous $NaHCO_3$ (1.5 mL) and ethyl acetate (1.5 mL) were added to extract the metal catalyst into the aqueous phase for protection of the GC. The resulting suspension was stirred for 20 min, after which the organic phase was separated and filtered through a short SiO_2 plug. Yields were determined from quantitative GC and NMR analyses *vs.* internal references.

Results and discussion

The metal precursors $Co_2(CO)_8$ and $[(AlCp^*)_4]$, $[Co(^iPr_2\text{-MeAMD})_2]$ and $[Me_2Al(^iPr_2\text{-MeAMD})]$ or $[Co(^iPr_2\text{-MeAMD})_2]$ and $[(AlCp^*)_4]$ were suspended in the dried $[BMIm]NTf_2$ IL for at least 24 h under an argon atmosphere to achieve a fine dispersion. Furthermore, the single-source precursor $[Cp^*Co(\mu\text{-H})(Al(\kappa^2\text{-}(CH_2SiMe_2)NSiMe_3)(btsa))]$ with a specific metal ratio and a Co–Al bond was suspended in $[BMIm]NTf_2$ overnight. The NP synthesis in IL was achieved by microwave irradiation using a power of 50 W to give an approximate temperature of 230 °C in the reaction mixture for 30 min (Scheme 5). A black NP dispersion was reproducibly obtained by decomposition of the organometallic precursors in the IL. Thermogravimetric analysis (TGA) revealed the full decomposition of the organometallic precursors at temperatures between 83 °C and 95 °C (Table S1 and Fig. S6, ESI†), whereas the $[BMIm]NTf_2$ IL decomposes at a temperature higher 424 °C (Fig. S2, ESI†). Based on the TGA measurements, a temperature of 230 °C was selected for all microwave-assisted thermal NP syntheses to achieve complete decomposition of the precursors and keep the formation of by-products as low as possible. At 230 °C, no IL decomposition was seen by TGA, ^{1}H- and ^{19}F-NMR, even by holding the temperature for 8 h (Fig. S3–S5, ESI†).

The morphology, crystalline phase, size and size dispersion of the purified Co/Al-nanoalloys were analyzed by TEM and SAED, together with HAADF-STEM and (HR-)XPS. The characterization was completed by EDX (in combination with TEM or EDX mapping with STEM) to determine the qualitative metal composition. Each sample was analyzed on a large scale and TEM images were taken from different positions on the grid to ensure the representative nature of the chosen particle ensemble. Small Co/Al-NPs with an average size between 2 nm (NP3) and 5 nm (NP4) and small size dispersions of ± 0.2–1 nm were readily obtained, according to the TEM analysis (Table 1).

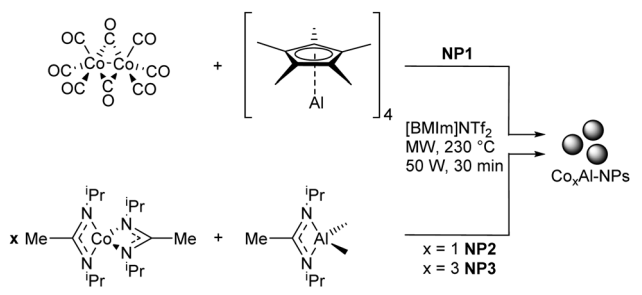

Scheme 5 Synthesis of Co/Al-NPs from $Co_2(CO)_8$ and $[(AlCp^*)_4]$ (NP1) or from $[Co(^iPr_2\text{-MeAMD})_2]$ and $[Me_2Al(^iPr_2\text{-MeAMD})]$ in different molar ratios (NP2 and NP3) by microwave (MW)-assisted thermal decomposition in $[BMIm]NTf_2$.

The decomposition of $[Co(^iPr_2\text{-MeAMD})_2]$ and $[(AlCp^*)_4]$ in $[BMIm]NTf_2$ (NP5) resulted in monometallic Co-NPs with an average size of 10 ± 3 nm, besides ill-defined amorphous Al (Fig. S21–S23, ESI†). The formation of Al-fluorides or oxyfluorides was ruled out by XPS (see below). Also for the synthesized single-source precursor $[Cp^*Co(\mu\text{-H})(Al(\kappa^2\text{-}(CH_2SiMe_2)NSiMe_3)(btsa))]$ in $[BMIm]NTf_2$ (NP6) only monometallic Co-NPs with average size of 26 ± 6 nm could be observed (Table S4 and Fig. S24–S26, ESI†). Pure Co-NPs (NP7) were synthesized from $[Co(^iPr_2\text{-MeAMD})_2]$ in $[BMIm]NTf_2$ for the investigation of the influence of aluminum on the catalytic activity of the Co/Al-NPs (NP2 and NP3). Further information is given in the ESI† (Fig. S12–S17).

Thermal decomposition of $Co_2(CO)_8$ and $[(AlCp^*)_4]$

For the synthesis of the CoAl-NPs (NP1), small NPs with an average size of 3.0 ± 0.5 nm were obtained. Most of the NPs were immobilized on an amorphous background (Fig. 1). The only crystalline phase in the NPs was identified by SAED to be face-centered cubic (fcc) CoAl (Fig. S9, ESI†). The SAED patterns were measured at different positions on the TEM grid to ensure the crystalline phase identity within the sample. EDX mapping in STEM indicated the presence of aluminum in the background and also in the areas around the NPs, whereas cobalt was only localized in the large NPs (orange window in Fig. 1). CoAl-NPs of 3 nm are not clearly visible in the EDX map (map size ~50 nm). The map shows obviously 20 nm large Co particles. The sampling of the map is too coarse to clearly image small NPs. Thus, the small CoAl-NPs appear as a diffuse background surrounding the large Co particles. Furthermore, EDX spectra were measured in TEM mode to determine the element composition over a larger segment (Fig. S10, ESI†). The TEM-EDX analysis suggests a significant compositional variation of Co : Al molar ratios ranging between 1 : 1 and 1 : 2 (±10 at% rel. error) at four different places on the TEM grid.

Additionally, the signals of oxygen and sulfur in all the EDX spectra indicate the presence of residual IL. XPS analysis of NP1 was carried out for further element composition investigations (Fig. 2 and Table 2). The survey spectrum identified aluminum, carbon, nitrogen, oxygen, fluorine, and cobalt (Fig. S11, ESI†). Nitrogen and fluorine indicate the presence of residual $[BMIm]NTf_2$ on the nanoparticle surface. HR-XPS were measured from aluminum, oxygen, fluorine and cobalt. The HR-XP spectra of the F 1s peak identified, as assumed before, organic fluorine from the IL at 690 eV but also small amounts of inorganic fluoride, presumably cobalt fluoride at 686 eV (Table 2 and Fig. 2).[76] Thus, the IL can also take part in the metal precursor decomposition by serving as a fluoride source. According to ion chromatography (IC), the IL contains only a very small amount of fluoride ions (< 1 ppm). Hence, only the bis(trifluoromethylsulfonyl)imide (triflimide) anion can be the fluoride source.[77,78]

Table 1 M-NP size determination for Co/Al-NPs[a]

Batch	Precursor	Co : Al[b]	Crystalline phase[c]	TEM ∅[d,e] [nm]
NP1	$Co_2(CO)_8$[$(AlCp^*)_4$]	1 : 1	CoAl	3.0 ± 0.5
NP2	[$Co(^iPr_2$-MeAMD$)_2$] [$Me_2Al(^iPr_2$-MeAMD)]	1 : 1	CoAl	3 ± 1
NP3	[$Co(^iPr_2$-MeAMD$)_2$] [$Me_2Al(^iPr_2$-MeAMD)]	3 : 1	Co_3Al	2.0 ± 0.2
NP4	[$Co(^iPr_2$-MeAMD$)_2$] [$Me_2Al(^iPr_2$-MeAMD)]	1.5 : 1	CoAl/Co_3Al	5 ± 1
NP5	[$Co(^iPr_2$-MeAMD$)_2$] [$(AlCp^*)_4$]	1 : 1	Co	10 ± 3
NP6	[Cp*Co(μ-H)(Al(κ^2-$(CH_2SiMe_2)NSiMe_3$)(btsa))]	—	Co	26 ± 6
NP7	[$Co(^iPr_2$-MeAMD$)_2$]	—	Co	3 ± 1

[a] 0.5/1.0 wt% M-NP/IL dispersions obtained by microwave-assisted heating for 30 min at 230 °C. [b] Applied molar ratio of precursors in dual-source precursor systems. [c] The crystalline phase of the NPs was determined by SAED. Non-crystalline phases are not identified by this technique. [d] Average diameter (∅). [e] See Experimental section for TEM measurement conditions; at least 100 particles were used for the size analysis.

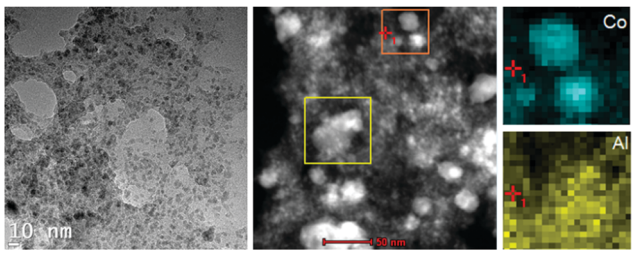

Fig. 1 TEM image (left), HAADF-STEM image (middle) and EDX-mapping (right) of cobalt (blue) and aluminum (yellow) in NP1 obtained by thermal decomposition of $Co_2(CO)_8$ and [$(AlCp^*)_4$] in [BMIm]NTf_2. The orange window in the HAADF-STEM image displays the area of EDX mapping. The yellow window displays the reference window, to see possible movement of the sample during the EDX mapping. See Fig. S8, ESI† for further TEM images and histogram of the particle size distribution.

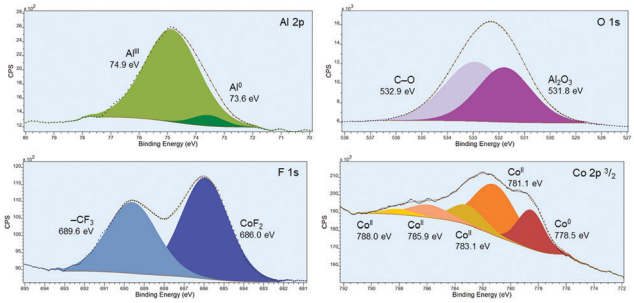

Fig. 2 HR-XPS of sample NP1 (0.5 wt% CoAl-NPs in [BMIm]NTf_2 from $Co_2(CO)_8$ and [$(AlCp^*)_4$]). HR-spectra of Al 2p, O 1s, F 1s and Co $2p_{3/2}$.

The analysis of the IL by NMR after the NP synthesis, with only traces of metal fluoride formed, gave no indication of its decomposition because of the trace amounts.[76] The O 1s orbital indicates two different oxygen species (Table 2 and Fig. 2). The first species at 532 eV can ascribed to Al_2O_3 and the second species at 533 eV to organic C–O.[79] The oxidation of the aluminum can be confirmed by the Al 2p orbital. The binding energy at 75 eV indicates an Al^{III} species.[80] AlF_3 would be located at higher binding energies around 78 eV.[81] Whereas Al_2O_3 and $Al(OH)_3$ are localized at around 74 eV.[81] Short contact with air during sample transfer to the XPS instrument could not be avoided and may have led to surface oxidation. The oxidation of Co and Al will be discussed later with regard to

Table 2 Comparison of XPS binding energies in sample NP1 in [BMIm]NTf_2[a]

XPS signal	NP1 deconvoluted bands	Characteristic regions[77,80–84]
Co $2p_{3/2}$ [eV]	778.5 (23%) 781.1–788.0 (77%)	Co^0 778.1–783.1 CoO 780.0–786.0 Co_3O_4 779.6–789.5 CoF2 780.9
F 1s [eV]	686.0 (57%) 689.6 (43%)	F^{-I} 684–685.5 F^0 688–689
O 1s [eV]	531.8 (44%) 532.9 (56%)	O^{-II} 529–530 O^{-II} in $Co^{+II/+III}$-oxide 530–532.9 O^0 531.5–533
Al 2p [eV]	73.6 (6%) 74.9 (94%)	Al^0 72.7 Al_2O_3 74.1 $AlOF_x$ 75.9 AlF_3 78.1

[a] XPS was performed with purified M-NPs. The NP-IL dispersion was washed several times with 2 mL acetonitrile each to remove the IL. The resulting material was dried under high vacuum until a black powder could be obtained.

possible passivation by aluminum. The quantification of cobalt and aluminum over the entire sample gave a Co : Al molar ratio of 1 : 1.

Altogether the sample NP1 shows the presence of crystalline CoAl-NPs on an amorphous alumina (Al_2O_3) background together with amorphous Co-oxide nanoparticles, the XPS-elucidated formation of alumina and Co-oxide is most likely due to the oxidation of metal species, as described in the literature and will be discussed later using the XPS results.[25,82] Thus, we interpreted the reaction product as a mixture of CoAl, Co and Al nanoparticles, with the latter being easily and rapidly oxidized. The synthesis of phase-pure Co/Al-NPs, that is, without the simultaneous formation of Co-NPs and Al_2O_3, may be difficult to achieve by this wet-chemical synthetic route.

Thermal decomposition of [$Co(^iPr_2$-MeAMD$)_2$] and [$Me_2Al(^iPr_2$-MeAMD)]

The thermal decomposition of [$Co(^iPr_2$-MeAMD$)_2$] and [$Me_2Al(^iPr_2$-MeAMD)] in various molar ratios in [BMIm]NTf_2 at 230 °C using a power of 50 W for 30 min led to the formation of small CoAl-NPs (NP2) and Co_3Al-NPs (NP3) with an average size of 2.0 ± 0.2 nm and 3 ± 1 nm. As can be seen for the

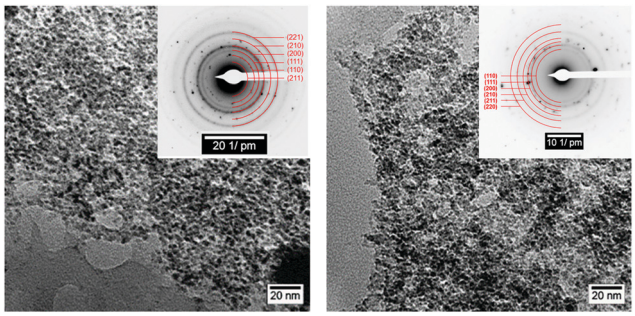

Fig. 3 HR-TEM images and SAEDs of fcc CoAl (NP2) and fcc Co_3Al (NP3) from $[Co(^iPr_2\text{-MeAMD})_2]$ and $[Me_2Al(^iPr_2\text{-MeAMD})]$ in $[BMIm]NTf_2$ ($CoAl$[85] (left) and Co_3Al[86] (right) reference reflexes in red, face-centered cubic (fcc) structures with space groups $Pm\bar{3}m$).

sample of NP4, the molar ratios of the precursors must be exactly 1 : 1 or 3 : 1 for the synthesis of CoAl- or Co_3Al-NPs. At a Co : Al precursor ratio of 1.5 : 1, a mixture of CoAl and Co_3Al-NPs was obtained (Table 1 and Fig. S18–S20, ESI†).

A high degree of agglomeration was observed for both composites. Furthermore, impurities as an amorphous background could be observed. The SAED patterns indicate the formation of crystalline fcc CoAl for NP2 and fcc Co_3Al for NP3. We noted that Co_3Al as nanoparticles was hitherto unknown. The SAED patterns were measured at different positions on the TEM grid to ensure crystalline phase identity within the sample.

The element compositions were determined by EDX (in combination with TEM) at three different positions. The TEM-EDX analysis suggests an excess of aluminum for NP2 (1 : 2, 2 : 3, and 1 : 3). This aluminum excess is derived from the presence of aluminum in the amorphous background, as described for NP1. For NP3 the TEM-EDX spectra indicate an excess of cobalt (5 : 1, 5 : 1, and 3 : 1) and indicate that cobalt is present in the amorphous impurities. In both samples NP2 and NP3, impurities of sulfur, carbon and oxygen from the IL were identifiable. It was not possible to identify the amorphous background. The TEM-EDX image only indicates the presence of aluminum in the background. Thus, different Co_xAl_y or Al phases are conceivable. However, it was not possible to synthesize Co/Al-NPs without this background irrespective of which precursors were used (Table 1). Again, it is evident that the synthesis of phase-pure Co/Al-NPs *via* a wet-chemical synthetic route remains a challenge.

XPS analysis was used to verify the element compositions of the samples (Table 3 and Fig. 4, 5). Both samples showed the partial oxidation of cobalt (13% Co^0 for NP2 and 9% Co^0 for NP3) and aluminum caused by their contact with air during the sample preparation. The quantification of cobalt and aluminum over the entire sample gave a Co : Al molar ratio of 1 : 1 for NP2 and 3 : 1 for NP3. HR-XPS of Al 2p indicates the oxidation of Al^0 to Al^{III}. Particularly Al_2O_3 is a possibility, while the presence of AlF_3 and $AlOF_x$ can be excluded (Table 3 and Fig. 4, 5). The XPS results indicate a correlation between the oxidation state of cobalt and the molar ratio of cobalt to aluminum in the NPs (Fig. 6).

Table 3 Comparison of the XPS binding energies in samples NP2 and NP3 in $[BMIm]NTf_2$[a]

XPS signal	NP2 deconvoluted bands	NP3 deconvoluted bands	Characteristic regions[77,80–82,84]
Co $2p_{3/2}$	778.0 (13%) 780.7–787.2 (87%)	779.4 (9%) 780.9–787.3 (91%)	Co^0 778.1–783.1 CoO 780.0–786.0 Co_3O_4 779.6–789.5
F 1s	685.1 (86%) 688.2 (14%)	—	F^{-I} 684–685.5 F^0 688–689
O 1s	531.1 (100%)	530.0 (45%) 531.6 (55%)	O^{-II} 529–530 $Co^{+II/+III}$ 530–532.9 O^0 531.5–533
Al 2p	73.3 (16%) 73.9 (84%)	71.2 (6%) 73.0 (94%)	Al^0 72.7 Al_2O_3 74.1 AlF_3 78.1

[a] XPS was performed with purified M-NPs. The NP-IL dispersion was washed several times with 2 mL acetonitrile each to remove the IL. The resulting material was dried under high vacuum until a black powder was obtained.

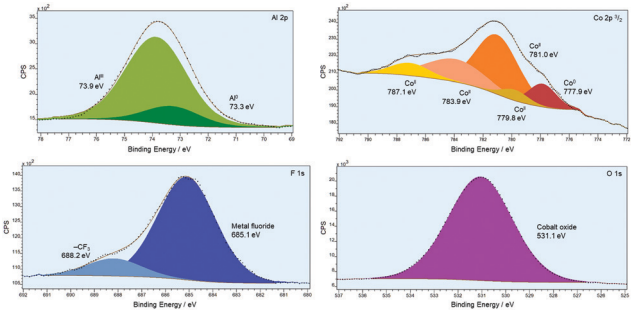

Fig. 4 HR-XPS of sample NP2 (1.0 wt% CoAl-NPs from $[Co(^iPr_2\text{-MeAMD})_2]$ and $[Me_2Al(^iPr_2\text{-MeAMD})]$ in $[BMIm]NTf_2$). HR-spectra of Al 2p, Co $2p_{3/2}$, F 1s and O 1s.

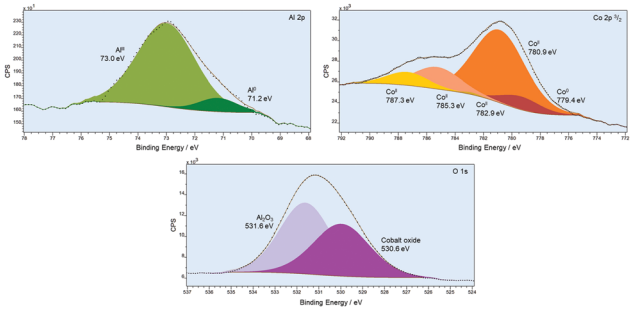

Fig. 5 HR-XPS of sample NP3 (1.0 wt% Co_3Al-NPs from $[Co(^iPr_2\text{-MeAMD})_2]$ and $[Me_2Al(^iPr_2\text{-MeAMD})]$ in $[BMIm]NTf_2$). HR-spectra of Al 2p, Co $2p_{3/2}$ and O 1s.

The binding energy for the Co $2p_{3/2}$ orbital of around 779 eV is indicative of a Co^0 species. Co^{+II}/Co^{+III} species occur at binding energies of 780–782 eV. A differentiation between CoO and Co_3O_4 is not possible because there is no significant difference in the binding energies between CoO, $Co(OH)_2$, Co_3O_4 and $CoAl_2O_4$ of Co $2p_{3/2}$.[87] The relative amount of Co^0

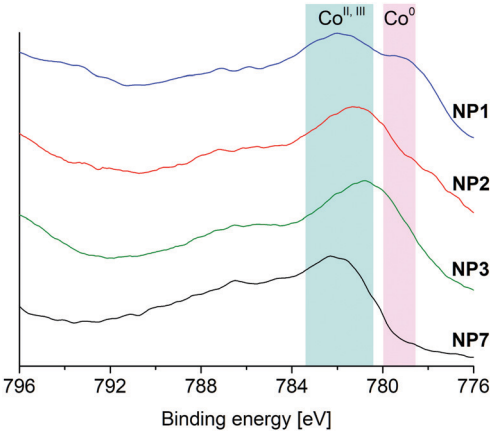

Fig. 6 Comparison of the HR-spectra of Co $2p_{3/2}$ of NP1 (blue), NP2 (red), NP3 (green) and NP7 (black) in the range of 776 eV to 794 eV.

seems to decrease when going from CoAl species (in samples NP1 and NP2) over Co_3Al (sample NP3) to neat Co (sample NP7). The latter has almost no signal intensity at around 779 eV. It is evident that samples NP1 to NP3 show a significant oxidation of cobalt caused by the unavoidable contact with air during the sample preparation for XPS.[88]

The striking difference is the full oxidation of what should have been pure Co-NPs in sample NP7. This suggests a protection or oxygen scavenger effect of the easier to oxidize aluminum content in samples NP1 to NP3 upon the short air contact during sample transfer to the XP spectrometer.[25] Further, comparing the "CoAl" samples NP1 and NP2 with the "Co_3Al" sample NP3, there is also a larger relative Co^0 proportion in the former. This supports the aluminum scavenger effect since samples NP1 and NP2 also contain an equimolar amount of aluminum, whereas NP3 has only one Al for three Co equivalents.

Hydrogenation reaction with Co-, CoAl- and Co_3Al-NPs

Cobalt-based catalysts are well known in catalytic hydrogenation reactions.[63–65] Several reactions can be catalyzed, such as the hydrogenation of C=O,[59,89–92] C=N,[59,91–95] and C=C.[59,92,93,96–98] For example, Beller and co-workers reported N-graphitic-modified Co-NPs for the selective semi-hydrogenation of alkynes (1 mol% Co-catalyst, 30 bar H_2, 120 °C in acetonitrile).[64] Herein, we applied the prepared Co- and Co/Al-NP samples NP7 (Co), NP2 (CoAl), and NP3 (Co_3Al) for the hydrogenation of alkenes and alkynes. NP7 in IL showed low catalytic activity in the hydrogenation of the model substrate phenylacetylene (Table 4 and Fig. S5, S7, ESI†). Therefore, the NPs were applied under IL-free conditions by washing the freshly prepared NP@IL several times with acetonitrile to remove [BMIm]NTf_2, followed by high-vacuum solvent evaporation. However, even with extensive washing it was difficult to remove the directly adhering IL (monolayer) on the NP surface. The signals in the EDX spectra for sulfur and fluorine and in the XPS for CF_3 confirm residual IL. The SAED patterns indicate the formation of crystalline fcc CoAl for NP2 and fcc Co_3Al for NP3 (Fig. 3). Powder X-ray diffraction yielded no diffractograms probably due to the small nanoparticle sizes. The aluminum-free Co-NPs (NP7) were inactive even under harsh conditions (80 bar H_2, 80 °C, Table 4, entry 2), whereas the CoAl- and Co_3Al-NPs under these same conditions gave complete conversions, albeit with low chemoselectivities (Table 4, entries 5 and 10, respectively). To apply milder reaction conditions, diisobutylaluminium hydride (DIBAL-H) was used as a co-catalyst to enhance the catalytic activity of the Co-NPs, most likely as a consequence of cobalt oxide reduction to cobalt(0) on the surface of the nanoparticles.[59,91,95,99–102]

DIBAL-H itself, showed no significant catalytic activity under the same conditions (Table 4, entry 15).

Table 4 Catalyst screening of NP7 (Co), NP2 (CoAl), NP3 (Co_3Al) and NP7-IL (Co-NP in IL)

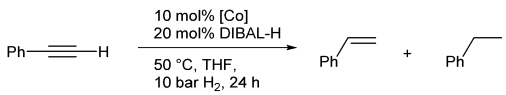

Entry	Catalyst	Additive	T [h]	Conditions[a]	Conversion [%]	Styrene [%]	Ethyl benzene [%]
1	10 mol% NP7	—	24	A	0	0	0
2		—	24	B	<5	1	0
3		20 mol% DIBAL-H	24	A	46[b]	34	4
4	10 mol% NP2	—	24	A	<5	2	0
5		—	24	B	>99	56	43
6		20 mol% DIBAL-H	24	A	>99	2	96
7	5 mol% NP2	10 mol% DIBAL-H	24	C	>99	4	91
8			6	C	63	55	6
9	10 mol% NP3	—	24	A	<5	3	0
10		—	24	B	>99	85	15
11		20 mol% DIBAL-H	24	A	>99	6	96
12	5 mol% NP3	10 mol% DIBAL-H	24	C	>99	2	97
13			6	C	83	72	9
14	0.1 mL NP7 in IL	—	24	D	0	0	0
15	—	10 mol% DIBAL-H	6	C	<5	1	0

General: The NP-IL dispersion was washed several times with 2 mL acetonitrile each to remove the IL. The resulting material was dried under high vacuum until a black powder was obtained, which was used as the (pre-)catalyst. [a] Conditions: 0.2 mmol alkyne in 0.5 mL THF. [A] 50 °C, 10 bar H_2, THF. [B] 80 °C, 80 bar H_2, THF. [C] 30 °C, 2 bar H_2, THF. [D] 50 °C, 20 bar H_2, hexane. [b] Trimerization as a side reaction.

Upon the addition of 10 mol% DIBAL-H, NP7 was converted to an active hydrogenation catalyst of phenylacetylene, which afforded styrene (34%) and ethyl benzene (4%) at 50 °C and 10 bar H_2. Traces of the [2+2+2]-cyclotrimerization products were also formed.[103–108] A similar activation by the hydride reagent DIBAL-H was observed with NP2 and NP3 (Table 4, entries 6–8 and 11–13, respectively). Although the conversion of phenylacetylene was low with catalytic NP2 and NP3 at 50 °C, 10 bar H_2 without DIBAL-H, near quantitative amounts of alkane were formed after NP activation with DIBAL-H under the same conditions. Both hydrogenations could also be performed under very mild conditions (2 bar H_2, 30 °C, Table 4, entries 7, 8 and 12, 13).

The samples withdrawn after 6 h from the reaction showed the semi-hydrogenation product styrene as the major component compared to the final alkane ethylbenzene (Table 4, entries 8 and 13). It is likely that the hydrogenation is a two-step process with the semi-hydrogenation product styrene formed first and presumably in a faster reaction step. Styrene is then independently hydrogenated to ethylbenzene, which takes a longer time to run to completion.

A series of alternative reductants were tested as co-catalysts (Tables S6 and S10, ESI†). $LiAlH_4$ showed comparable reactivity to DIBAL-H; BH_3·THF and NaH gave lower conversions. Lower amounts of DIBAL-H resulted in lower catalytic activities (Table S10, ESI†). In summary, the highest catalytic activity for the hydrogenation of phenylacetylene was achieved with the combinations of DIBAL-H and NP2 or NP3 in THF (Table 4, entries 7, 8 and 12, 13), respectively.

Subsequently, we explored the scope of this hydrogenation protocol with NP3 (Fig. 7). The observed chemoselectivities were strongly dependent on the functional groups present in the substrates and the reaction times. Phenylacetylene, 3-methylphenylacetylene and 1-octyne cleanly afforded the corresponding alkanes. 4-Chlorophenylacetylene gave the alkene (alkene/alkane = 8 : 1), but underwent no competing hydrodehalogenation. Substrates with methoxy, carbonyl and amine moieties showed significantly lower conversion (Fig. 7). The internal alkyne phenylpropyne afforded 29% hydrogenation products, with 1-*Z*-phenyl-1-propene as the major product. The alkene α-methylstyrene showed very low conversion, which may be relevant in the context of chemoselective hydrogenations of alkynes over (sterically hindered) 1,1-substituted alkenes. Nitriles, ketones or nitro compounds showed no conversion to hydrogenated products, probably due to irreversible catalyst oxidation by the reduction-sensitive functional groups.

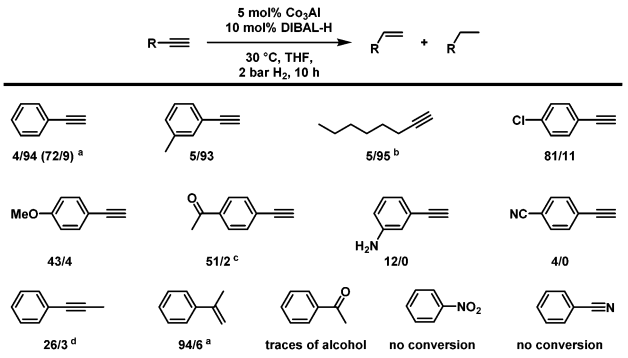

Fig. 7 Hydrogenation of alkynes, nitriles, ketones and nitro compounds with Co_3Al-NPs. The NP-IL dispersion was washed several times with 2 mL acetonitrile each to remove the IL. The resulting material was dried under high vacuum until a black powder was obtained. Standard conditions: 5 mol% NP3 (Co_3Al), 10 mol% DIBAL-H, 200 μmol substrate in 0.5 mL THF, 30 °C, 2 bar H_2, 10 h. Yield of alkene/yield of alkane. (a) 6 h reaction time. (b) Mixture of alkenes. (c) 5% of ketone reduction. (d) 6 h reaction time, 24% *Z*-alkene + 2% *E*-alkene.

Conclusions

The synthesis of the Co/Al nanoalloys CoAl and the previously unknown Co_3Al in nanoparticular form yielded NP diameters of less than 10 nm by microwave-assisted thermal decomposition in an ionic liquid. The dual-source precursor systems of various organometallic cobalt and aluminum complexes in the ionic liquid [BMIm]NTf_2 were used for the synthesis of Co/Al-NPs in different ratios. The metal precursors $Co_2(CO)_8$ and $[(AlCp^*)_4]$ or $[Co(^iPr_2\text{-MeAMD})_2]$ and $[Me_2Al(^iPr_2\text{-MeAMD})]$ proved to be successful for the synthesis of the Co/Al nanoalloys. Whereas, the dual-source system of $[Co(^iPr_2\text{-MeAMD})_2]$ and $[(AlCp^*)_4]$ and also the single-source precursor $[Cp^*Co(\mu\text{-}H)(Al(\kappa^2\text{-}(CH_2SiMe_2)\text{-}NSiMe_3)(btsa))]$ led to the formation of monometallic Co-NPs. However, all the products showed impurities of amorphous aluminum species in the background of the Co/Al- or Co-NPs. Thus, admittedly, the phase-pure synthesis of Co/Al-NPs from a dual- or even a single-source precursor *via* a wet-chemical synthetic route remains an unresolved problem. It is still a challenge to avoid the concomitant formation of Co-NPs and Al_2O_3. Thereby, we noted that in the only other two reports on Co/Al-NPs, oxide byproducts (Al_2O_3)[28] or even fully oxidized $CoAlO_x$-NPs were formed.[68] The presence of dioxygen impurities seems very difficult to avoid, which together with the high oxophilicity of Co and Al metal then led to substantial oxidation products. This oxidation may not necessarily occur during the synthesis but during the necessary subsequent handling for analysis, where often an even short contact with air is unavoidable. For future work in this direction, other single-source precursors, synthetic conditions with reducing agents (which also act as oxygen scavengers), more stringent inert conditions also for analysis, and protection of the Co/Al-NPs by stabilizing capping agents (which may also block the access of O_2) may be routes to follow.

We examined the catalytic properties of the as-formed Co/Al-NPs in hydrogenation reactions. Both CoAl- (NP2) and Co_3Al-NPs (NP3) were effective catalysts for alkyne-to-alkane hydrogenation in the presence of DIBAL-H as a co-catalyst under mild conditions (2 bar H_2, 30 °C).

Further investigations can also focus on the synthesis of further Co/E nanoalloys (E = Ga and In) and the examination of their catalytic properties.

Conflicts of interest

There are no conflicts to declare.

Acknowledgements

This work has been supported by the German Science Foundation (DFG) within the priority program SPP 1708 "*Material Synthesis Near Room Temperature*" (grant Fi502/32-1/2 for RAF and grant JA 466/31-1/2 for CJ). The authors gratefully acknowledge technical assistance by the Max-Planck-Institut für Eisenforschung GmbH, Düsseldorf for TEM measurements.

Notes and references

1 F. Tao, S. Zhang, L. Nguyen and X. Zhang, *Chem. Soc. Rev.*, 2012, **41**, 7980–7993.
2 M. Fatmi, M. A. Ghebouli, T. Chihi, S. Boucetta and Z. K. Heiba, *Rom. J. Phys.*, 2011, **56**, 935–951.
3 J. Zhang, G. Chen, D. Guay, M. Chaker and D. Ma, *Nanoscale*, 2014, **6**, 2125–2130.
4 I. Favier, E. Teuma and M. Gomez, in *Nanocatalysis in Ionic Liquids*, ed. M. H. G. Prechtl, Wiley-VCH, Weinheim, 2017.
5 H. Lindlar, *Helv. Chim. Acta*, 1952, **35**, 446–450.
6 M. García-Mota, J. Gómez-Díaz, G. Novell-Leruth, C. Vargas-Fuentes, L. Bellarosa, B. Bridier, J. Pérez-Ramírez and N. Lópet, *Theor. Chem. Acc.*, 2011, **128**, 663–673.
7 G. Vilé, N. Almora-Barrios, S. Mitchell, N. López and J. Pérez-Ramírez, *Chem. – Eur. J.*, 2014, **20**, 5926–5937.
8 S. Nishimura, *Handbook of Heterogeneous Catalytic Hydrogenation for Organic Synthesis*, Wiley, New York, 2001, p. 148.
9 M. Armbrüster, G. Wowsnick, M. Friedrich, M. Heggen and R. Cardoso-Gil, *J. Am. Chem. Soc.*, 2011, **133**, 9112–9118.
10 W.-C. Liu, G. Melaet, W. T. Ralston, S. Alayoglu, Y. Horowitz, R. Ye, T. Hurlburt, B. Mao, E. Crumlin, M. Salmeron and G. A. Somorjai, *Catal. Lett.*, 2016, **146**, 1574–1580.
11 S. Alayoglu, S. K. Beaumont, G. Melaet, A. E. Lindeman, N. Musselwhite, C. J. Brooks, M. A. Marcus, J. Guo, Z. Liu, N. Kruse and G. A. Somorjai, *J. Phys. Chem. C*, 2013, **117**, 21803–21809.
12 S. Alayoglu, S. K. Beaumont, F. Zheng, V. V. Pushkarev, H. Zheng, V. Iablokov, Z. Liu, J. Guo, N. Kruse and G. A. Somorjai, *Top. Catal.*, 2011, **54**, 778–785.
13 K. Schütte, A. Doddi, C. Kroll, H. Meyer, C. Wiktor, C. Gemel, G. van Tendeloo, R. A. Fischer and C. Janiak, *Nanoscale*, 2014, **6**, 5532–5544.
14 K. Schütte, H. Meyer, C. Gemel, J. Barthel, R. A. Fischer and C. Janiak, *Nanoscale*, 2014, **6**, 3116–3126.
15 M. Armbrüster, K. Kovnir, M. Friedrich, D. Teschner, G. Wowsnick, M. Hahne, P. Gille, L. Szentmiklósi, M. Feuerbacher, M. Heggen, F. Girgsdies, D. Rosenthal, R. Schlögl and Y. Grin, *Nat. Mater.*, 2012, **11**, 690–693.
16 G. Ertl, H. Knozinger, F. Schuth and J. Weitkamp, *Handbook of heterogeneous catalysis*, Wiley-VCH, Chichester, 2008.
17 P. Xi, Y. Cao, F. Yang, C. Ma, F. Chen, S. Yu, S. Wang, Z. Zeng and X. Zhang, *Nanoscale*, 2013, **5**, 6124–6130.
18 D. O. Silva, L. Luza, A. Gual, D. L. Baptista, F. Bernardi, M. J. M. Zapata, J. Morais and J. Dupont, *Nanoscale*, 2014, **6**, 9085–9092.
19 C. Dietrich, G. Uzunidis, Y. Träutlein and S. Behrens, *J. Visualized Exp.*, 2018, **138**, e58058.
20 W. T. Ralston, W.-C. Liu, S. Alayoglu and G. Melaet, *Top. Catal.*, 2018, **61**, 1002–1015.
21 M. M. van Schooneveld, C. Campos-Cuerva, J. Pet, J. D. Meeldijk, A. Meijerink, B. H. Erné and M. F. de Groot, *J. Nanopart. Res.*, 2012, **14**, 991–1003.
22 M. Sankar, N. Dimitratos, P. J. Miedziak, P. P. Wells, C. J. Kiely and G. J. Hutchings, *Chem. Soc. Rev.*, 2012, **41**, 8099–8139.
23 D. Martin Alonso, S. G. Wettstein and J. A. Dumesic, *Chem. Soc. Rev.*, 2012, **41**, 8075–8098.
24 R. Ferrando, J. Jellinek and R. L. Johnston, *Chem. Rev.*, 2008, **108**, 847–910.
25 M. Cokoja, H. Parala, A. Birkner, R. A. Fischer, O. Margeat, D. Ciuculescu, C. Amiens, B. Chaudret, A. Falqui and P. Lecante, *Eur. J. Inorg. Chem.*, 2010, 1599–1603.
26 M. Cokoja, H. Parala, A. Birkner, O. Shekhah, M. W. E. van Berg and R. A. Fischer, *Chem. Mater.*, 2007, **19**, 5721–5733.
27 M. Cokoja, H. Parala, M. K. Schröter, A. Birkner, M. W. E. van den Berg, W. Grünert and R. A. Fischer, *Chem. Mater.*, 2006, **18**, 1634–1642.
28 M. Cokoja, B. J. Jagirdar, H. Parala, A. Birkner and R. A. Fischer, *Eur. J. Inorg. Chem.*, 2008, 3330–3339.
29 W. Ostwald, *Z. Phys. Chem.*, 1901, **37**, 385.
30 W. Ostwald, *Lehrbuch der Allgemeinen Chemie*, Engelmann, Leipzig, 1896.
31 P. S. Campbell, M. H. G. Prechtl, C. C. Santini and P.-H. Haumesser, *Curr. Org. Chem.*, 2013, **17**, 414–429.
32 D. Freudenmann, S. Wolf, M. Wolff and C. Feldmann, *Angew. Chem., Int. Ed.*, 2011, **50**, 11050–11060.
33 E. Ahmed, J. Breternitz, M. F. Groh and M. Ruck, *CrystEngComm*, 2012, **14**, 4874–4885.
34 L. Schmolke, S. Lerch, M. Bülow, M. Siebels, A. Schmitz, J. Thomas, G. Dehm, C. Held, T. Strassner and C. Janiak, *Nanoscale*, 2019, **11**, 4073–4082.
35 J. D. Scholten, B. C. Leal and J. Dupont, *ACS Catal.*, 2012, **21**, 184–200.
36 T. Dang-Bao, D. Pla, I. Favier and M. Gómez, *Catalysts*, 2017, **7**, 207–240.
37 P. Dash, N. A. Dehm and R. W. J. Scott, *J. Mol. Catal. A: Chem.*, 2008, **286**, 114–119.
38 C. Vollmer and C. Janiak, *Coord. Chem. Rev.*, 2011, **255**, 2039–2057.
39 H. Kaper, F. Endres, I. Djerdj, M. Antonietti, B. M. Smarsly, J. Maier and Y.-S. Hu, *Small*, 2007, **3**, 1753–1763.
40 M. Antonietti, D. Kuang, B. Smarsly and Y. Zhou, *Angew. Chem., Int. Ed.*, 2004, **43**, 4988–4992.
41 D. Marquardt and C. Janiak, *Nachr. Chem.*, 2013, **61**, 754–757.
42 J. Dupont and J. D. Scholten, *Chem. Soc. Rev.*, 2010, **39**, 1780–1804.
43 P. Wasserscheid and W. Keim, *Angew. Chem., Int. Ed.*, 2000, **39**, 3772–3789.
44 J. Dupont, *J. Braz. Chem. Soc.*, 2004, **15**, 341–350.
45 K. Schütte, J. Barthel, M. Endres, M. Siebels, B. Smarsly, J. Yue and C. Janiak, *ChemistryOpen*, 2017, **6**, 137–148.

46 A. Schmitz, K. Schütte, V. Ilievski, J. Barthel, L. Burk, R. Mülhaupt, J. Yue, B. Smarsly and C. Janiak, *Beilstein J. Nanotechnol.*, 2017, **8**, 2474–2483.
47 M. Siebels, L. Mai, L. Schmolke, K. Schütte, J. Barthel, J. Yue, J. Thomas, B. M. Smarsly, A. Devi, R. A. Fischer and C. Janiak, *Beilstein J. Nanotechnol.*, 2018, **9**, 1881–1894.
48 C. Vollmer, R. Thomann and C. Janiak, *Dalton Trans.*, 2012, **41**, 9722–9727.
49 C. Vollmer, E. Redel, K. Abu-Shandi, R. Thomann, H. Manyar, C. Hardacre and C. Janiak, *Chem. – Eur. J.*, 2010, **16**, 3849–3858.
50 D. Marquardt, C. Vollmer, R. Thomann, P. Steurer, R. Mülhaupt, E. Redel and C. Janiak, *Carbon*, 2011, **49**, 1326–1332.
51 R. Marcos Esteban, K. Schütte, D. Marquardt, J. Barthel, F. Beckert, R. Müllhaupt and C. Janiak, *Nano-Struct. Nano-Objects*, 2015, **2**, 28–34.
52 S. Schmidt, S. Schulz and M. Bolte, *Z. Anorg. Allg. Chem.*, 2009, **635**, 2210–2213.
53 B. S. Lim, A. Rahtu, J.-S. Park and R. G. Gordon, *Inorg. Chem.*, 2003, **42**, 7951–7958.
54 H. Li, D. B. Farmer, R. G. Gordon, Y. Lin and J. Vlassak, *J. Electrochem. Soc.*, 2007, **154**, 642–647.
55 J. P. Coyle, W. H. Monillas, G. P. Yap and S. T. Barry, *Inorg. Chem.*, 2008, **47**, 683–689.
56 J. Krämer, E. Redel, R. Thomann and C. Janiak, *Organometallics*, 2008, **27**, 1976–1978.
57 E. Redel, J. Krämer, R. Thomann and C. Janiak, *J. Organomet. Chem.*, 2009, **694**, 1069–1075.
58 S. Sandl, F. Schwarzhuber, S. Pöllath, J. Zweck and A. Jacobi von Wangelin, *Chem. – Eur. J.*, 2018, **24**, 3403–3407.
59 R. Ferraccioli, D. Borovika, A.-E. Surkus, C. Kreyenschulte, C. Topf and M. Beller, *Catal. Sci. Technol.*, 2018, **8**, 499–507.
60 F. Michalek, A. Lagunas, C. Jimeno and M. A. Pericàs, *J. Mater. Chem.*, 2008, **18**, 4692–4697.
61 P. Jiang, X. Li, W. Gao, X. Wang, Y. Tang, K. Lan, B. Wang and R. Li, *Catal. Commun.*, 2018, **111**, 6–9.
62 C. Chen, Y. Huang, Z. Zhang, X.-Q. Dong and X. Zhang, *Chem. Commun.*, 2017, **53**, 4612–4615.
63 F. Chen, C. Kreyenschulte, J. Radnik, H. Lund, A.-E. Surkus, K. Junge and M. Beller, *ACS Catal.*, 2017, **7**, 1526–1532.
64 P. Büschelberger, E. Reyes-Rodriguez, C. Schöttle, J. Treptow, C. Feldmann, A. Jacobi von Wangelin and R. Wolf, *Catal. Sci. Technol.*, 2018, **8**, 2648–2653.
65 R. Xu, T. Xie, Y. Zhang and Y. Li, *Nanotechnology*, 2007, **18**, 055602.
66 R. B. N. Baig, S. Verma, R. S. Varma and N. Nadagouda, *ACS Sustainable Chem. Eng.*, 2016, **4**, 1661–1664.
67 L. Wang, L. Wang, J. Zhang, X. Liu, H. Wang, W. Zhang, Q. Yang, J. Ma, X. Dong, S. J. Yoo, J.-G. Kim, X. Meng and F.-S. Xiao, *Angew. Chem., Int. Ed.*, 2018, **57**, 6104–6108.
68 H. Bürger and U. Wannagat, *Monatsh. Chem.*, 1963, **94**, 1007–1012.
69 C. Ganesamoorthy, S. Loerke, C. Gemel, M. Winter, P. Jerabek, G. Frenking and R. A. Fischer, *Chem. Commun.*, 2013, **49**, 2858–2860.
70 M. Luysberg, M. Heggen and K. Tillmann, *J. Large Scale Res. Facil.*, 2016, **2**, 138.
71 A. Thust, J. Barthel and K. Tillmann, *J. Large Scale Res. Facil.*, 2016, 41.
72 S. Schmidt, S. Schulz, D. Blaeser, R. Boese and M. Bolte, *Organometallics*, 2010, **29**, 6097–6103.
73 M. P. Coles, D. C. Swenson and R. F. Jordan, *Organometallics*, 1997, **16**, 5183–5194.
74 J. Weßing, C. Göbel, B. Weber, C. Gemel and R. A. Fischer, *Inorg. Chem.*, 2017, **56**, 3517–3525.
75 S. Wegner, C. Rutz, K. Schütte, J. Barthel, A. Bushmelev, A. Schmidt, K. Dilchert, R. A. Fischer and C. Janiak, *Chem. – Eur. J.*, 2017, **23**, 6330–6340.
76 Z.-W. Fu, C.-L. Li, J. Ma, Y. Wang and Q.-Z. Qin, *J. Electrochem. Soc.*, 2015, **152**, E50–E55.
77 M. G. Freire, C. M. S. S. Neves, I. M. Marrucho, J. A. P. Coutinho and A. M. Fernandes, *J. Phys. Chem. A*, 2010, **114**, 3744–3749.
78 C. Rutz, L. Schmolke, V. Gvilava and C. Janiak, *Z. Anorg. Allg. Chem.*, 2017, **643**, 130–135.
79 G. Beamson and D. Briggs, *High Resolution XPS of Organic Polymers*, The Scienta ESCA300 Database Wiley Interscience, Chichester, 1992.
80 B. R. Strohmeier, *Surf. Interface Anal.*, 1990, **15**, 51–56.
81 O. Böse, E. Kemnitz, A. Lippitz and W. E. S. Unger, *Appl. Surf. Sci.*, 1997, **120**, 181–190.
82 T. Liu, Y. Pang, H. Kikuchi, Y. Kamada and S. Takahashi, *J. Mater. Chem. C*, 2015, **3**, 6232–6239.
83 R. Ramos, G. Cunge, P. Pelissier and O. Joubert, *Plasma Sources Sci. Technol.*, 2007, **16**, 711–715.
84 M. C. Biesinger, B. P. Payne, A. P. Grosvenor, L. W. M. Lau, A. R. Gerson and R. St. C. Smart, *Appl. Surf. Sci.*, 2011, **257**, 2717–2730.
85 S. N. Hosseini, T. Mousavi, F. Karimzadeh and M. H. Enayati, *J. Mater. Sci. Technol.*, 2011, **27**, 601–606.
86 M. Ellner, S. Kek and B. Predel, *J. Alloys Compd.*, 1992, **189**, 245–248.
87 A. A. Khassin, T. M. Yurieva, V. V. Kaichev, V. I. Bukhtiyarov, A. A. Budneca, E. A. Paushtis and V. N. Parmon, *J. Mol. Catal. A: Chem.*, 2001, **175**, 189–204.
88 H. Bönnemann, W. Brijoux, R. Brinkmann, N. Matoussevitch, N. Walföfner, N. Palina and H. Modrow, *Inorg. Chim. Acta*, 2003, **350**, 617–624.
89 S. Rösler, J. Obenauf and R. Kempe, *J. Am. Chem. Soc.*, 2015, **137**, 7998–8001.
90 F. Chen, C. Topf, J. Radnik, C. Kreyenschulte, H. Lund, M. Schneider, A.-E. Surkus, L. He, K. Junge and M. Beller, *J. Am. Chem. Soc.*, 2016, **138**, 8781–8788.
91 G. Zhang, B. L. Scott and S. K. Hanson, *Angew. Chem., Int. Ed.*, 2012, **51**, 12102–12106.
92 D. Gärtner, A. Welther, B. R. Rad, R. Wolf and A. Jacobi von Wangelin, *Angew. Chem., Int. Ed.*, 2014, **53**, 3722–3726.
93 F. Chen, A.-E. Surkus, L. He, M.-M. Pohl, J. Radnik, C. Topf, K. Junge and M. Beller, *J. Am. Chem. Soc.*, 2015, **137**, 11718–11724.
94 Z. Wie, Y. Chen, J. Wang, D. Su, M. Tang, S. Mao and Y. Wang, *ACS Catal.*, 2016, **6**, 5816–5822.

95 R. Adam, J. R. Cabrero-Antonino, A. Spannenberg, K. Junge, R. Jackstell and M. Beller, *Angew. Chem., Int. Ed.*, 2017, **56**, 3216–3220.
96 K. Tokmic, C. R. Markus, L. Zhu and A. R. Fout, *J. Am. Chem. Soc.*, 2016, **138**, 11907–11913.
97 R. P. Yu, J. M. Darmon, C. Milsmann, G. W. Margulieux, S. C. E. Stieber, S. DeBeer and P. J. Chirik, *J. Am. Chem. Soc.*, 2013, **135**, 13168–13184.
98 P. Büschelberger, D. Gärtner, E. Reyes-Rodriguez, F. Kreyenschmidt, K. Koszinowski, A. Jacobi von Wangelin and R. Wolf, *Chem. – Eur. J.*, 2017, **23**, 3139–3151.
99 J. Osuna, D. de Caro, C. Amiens, B. Chaudret, E. Snoeck, M. Respaud, J.-M. Broto and A. Fert, *J. Phys. Chem.*, 1996, **100**, 14571–14574.
100 F. K. Schmidt, Y. Titova, L. B. Belykh, V. A. Umanets and S. S. Khutsishvili, *Russ. J. Gen. Chem.*, 2012, **82**, 1334–1341.
101 T. Schwob and R. Kempe, *Angew. Chem., Int. Ed.*, 2016, **55**, 15175–15179.
102 R. V. Jagadeesh, K. Murugesan, A. S. Alshammari, H. Neumann, M.-M. Pohl, J. Radnik and M. Beller, *Science*, 2017, **358**, 326–332.
103 G. Domínguez and J. Pérez-Castells, *Chem. – Eur. J.*, 2016, **22**, 6720–6739.
104 P. R. Chopade and J. Louie, *Adv. Synth. Catal.*, 2006, **348**, 2307–2327.
105 N. Saino, D. Kogure and S. Okamoto, *Org. Lett.*, 2005, **14**, 3065–3067.
106 S. Saito and Y. Yamamoto, *Chem. Rev.*, 2000, **100**, 2901–2915.
107 M. Lautens, W. Klute and W. Tam, *Chem. Rev.*, 1996, **96**, 49–92.
108 N. Agenet, V. Gandon, K. P. C. Vollhardt, M. Malacria and C. Aubert, *J. Am. Chem. Soc.*, 2007, **129**, 8860–8871.

